

A novel hierarchical multiresolution framework using CutFEM

E. Mikaeili¹, S. Claus², P. Kerfriden^{1,3}

¹ Cardiff University, School of Engineering,
The Parade, CF243AA Cardiff, United Kingdom

² ONERA, 8 Chemin de la Hunière, 91120 Palaiseau, France

³MINES ParisTech, PSL Research University, MAT–Centre des Matériaux,
CNRS UMR 7633, BP 87 91003 Evry, France

Summary

In this paper, we propose a robust concurrent multiscale method for continuum-continuum coupling based on the cut finite element method. The computational domain is defined in a fully non-conforming fashion by approximate signed distance functions over a fixed background grid and decomposed into microscale and macroscale regions by a novel zooming technique. The zoom interface is represented by a signed distance function which is allowed to intersect the computational mesh arbitrarily. We refine the mesh inside the zooming region hierarchically for high-resolution computations. In the examples considered here, the microstructure can possess void, and hard inclusions and the corresponding geometry is defined by a signed distance function interpolated over the refined mesh. In our zooming technique, the zooming interface is allowed to intersect the microstructure interface in an arbitrary way. Then, the coupling between the subdomains is applied using Nitsche’s method across interfaces. This multiresolution framework proposes an efficient stabilized algorithm to ensure the stability of elements cut by the zooming and the microstructure interfaces. It is tested for several multiscale examples to demonstrate its robustness and efficiency for elasticity and plasticity problems.

Keywords: Concurrent Multiscale; Unfitted Multimesh; CutFEM; Nitsche; Plasticity

1 Introduction

Numerical analysis of heterogeneous materials such as composites are conventionally carried out with properties obtained from homogenization methods (see, e.g. [1, 2, 3]), passing data from small to large length scales wherein the macroscale properties are achieved by averaging stresses and strains over a periodic representative volume element (RVE). However, these homogenization methods suffer from drawbacks, including macroscopic uniformity and RVE periodicity assumptions. The uniformity assumption is not satisfied in critical regions of high gradients like interfaces, complex geometries with sharp angles, and plasticity and softening regions. The periodicity assumption is also not fulfilled when the material’s microstructure is nonuniform. In this context,

using full micro-scale models leads to accurate responses, but it is not tractable for large scale structures. These problems have been tackled effectively by concurrent multiscale methods [4, 5] that can bridge the microstructural and homogenized macro-scale descriptions. Domain partitioning in these multiscale methods distinguishes regions requiring different resolutions, zooming in for microscale modelling at critical regions, and using macroscale analysis elsewhere.

The major challenge with concurrent multiscale methods is adequately modelling the coupling between scales. To address this issue, two main categories of solutions are available. The first category is overlapping domain decomposition methods which are mainly convenient approaches to tackle the difficulties of coupling two scales with incompatible kinematics, for instance, the bridging domain method for coupling molecular dynamics with continuum [6, 7] and the quasicontinuum method for atomistic-continuum coupling [8, 9]. The Arlequin method [10] is another so-called overlapping technique that partitions the energy in the overlapping domain over the subdomains to enforce the compatibility of the mechanical states. This method has been applied successfully for coupling continuum-continuum [11, 12], discrete-continuum [13] and atomistic-continuum [14]. The second category is based on non-overlapping domain decomposition techniques that couple the two models over an interface, for instance, in the context of Mortar Method [15] which connects two scales in an average sense. In non-overlapping techniques, two models with or without different scales or physics are linked together. The restrictions imposed over the interface can be carried out either using Lagrange multipliers [16, 17, 18] or Nitsche's method [19, 20].

The geometric description in domain decomposition methods can be based on either conforming or non-conforming techniques. Employing conforming methods such as classical FEM [21] and Arbitrary Lagrangian Eulerian Methods [22] increase the computational preprocessing costs, particularly when the structure geometry is complex or time-dependent. On the contrary, non-conforming domain decomposition methods aim at not only decoupling the geometric description from the mesh for approximating solutions but also ensuring the stability of solvers. Implementing non-conforming techniques for domain decomposition methods can significantly simplify the mesh generation. The well-known examples of non-conforming methods are; extended finite element method (XFEM) [23], cut finite element method (CutFEM) [24], assumed enhanced strain (AES) method [25] and finite cell method (FCM) [26]. Using these methods in the context of domain decomposition methods requires robust numerical integration and stabilization techniques. This paper focuses on extending the CutFEM integration and stabilization algorithm for non-overlapping domain decomposition problems.

CutFEM technique, as a variation of XFEM, treats the elements with discontinuities by using overlapped fictitious domain technique combined with the ghost penalty regularization to decouple the geometry from meshing and also guarantee the solver stability. This method has been developed for problems in two-phase fluid flow [27, 28], multi-physics [29, 30] and contact mechanics [31, 32]. However, there are only a few extensions to multiscale and multiresolution methodologies in the literature. We refer to a multimesh framework suggested by [33, 34, 35] and a mixed multiscale proposed by [36], as examples of the non-overlapping and overlapping domain decomposition methods, respectively. The former method combines Nitsche's method with ghost penalty regularization [37] to alleviate the meshing burdensome of multi-component structures, which allows each part to own separate meshes and intersect and overlap each other arbitrarily, while the latter method uses ghost penalty regularization within a novel mixing framework to address the integration and stability issues.

This study proposes a novel multiresolution framework based on the CutFEM for multiscale modelling of heterogeneous structures with complex microstructures. The structures can possess

linear and nonlinear material properties. Within this framework, we first define regions of interest or "zooms" implicitly through level set functions interpolated over a fixed coarse mesh background. The corresponding interface can intersect the background mesh arbitrarily. Due to the necessity of high-resolution simulations inside the zooms, we refine the elements inside hierarchically. Then, another level set function is introduced to define the microstructure inside zoom, which is interpolated over the high-resolution mesh. The main novelty of the paper is in the way we treat the bilinear and linear forms of the cut elements by zoom and microstructure interfaces. We use Nitsche's method over the interfaces to glue different regions together. Then to guarantee the well-conditioning of the multiresolution system matrix and the stability of the solver, the cut elements are regularized with the ghost penalty technique.

The paper is outlined as follows. In section 2, we will present a concurrent multiscale formulation for linear elasticity and plasticity problems. Then we will discretize the multiscale formulation within the CutFEM algorithm. In section 3, the proposed multiscale framework will be tested for different heterogeneous structures.

2 Multiresolution finite element: zooming without meshing

2.1 Heterogeneous elasticity problem: strong form

2.1.1 Semi-discrete boundary value problem

To introduce the method, we consider a time-dependent elasticity problem for a two-phase composite material occupying domain $\Omega = \Omega^0 \cup \Omega^1$, where $\Omega^0 \cap \Omega^1 = \{\cdot\}$, in dimension $d \in \{2, 3\}$. In our presentation, Ω^0 corresponds to the matrix phase of the composite, and Ω^1 corresponds to an inclusion phase (ellipsoids). The semi-discrete problem of elasticity that we wish to solve is the following. Time interval $\mathcal{T} = [0, T]$ into N equally spaced time intervals. At discrete times in $\mathcal{T}_{\Delta T} = \{t_1 = \Delta T, t_2 = 2\Delta T, \dots, t_N = N\Delta T = T\}$, we look for displacement $u_n := \{u^{n,1}, u^{n,2}\} : \Omega^0 \times \Omega^1 \rightarrow \mathbb{R}^D \times \mathbb{R}^D$ satisfying,

$$\forall i \in \{0, 1\}, \quad \operatorname{div} \sigma^{i,n}(\nabla_s u^i) + f^n = 0 \quad \text{in } \Omega^i. \quad (1)$$

The boundary conditions of the elasticity problem are

$$\forall i \in \{0, 1\}, \quad u^{i,n} = u_d^n \quad \text{over } \partial\Omega_u \cap \partial\Omega^i \quad (2)$$

and

$$\forall i \in \{0, 1\}, \quad \sigma^i(\nabla_s u^{i,n}) \cdot n_{\partial\Omega} = t_d^n \quad \text{over } \partial\Omega_t \cap \partial\Omega^i \quad (3)$$

where $\partial\Omega = \partial\Omega_t \cup \partial\Omega_u$, $\partial\Omega_t \cap \partial\Omega_u = \{\cdot\}$. Fields f^n , u_d^n and t_d^n are given time-discrete fields. $n_{\partial\Omega}$ denotes the outer normal to the boundary.

In this contribution, domain Ω^0 and Ω^1 are implicitly defined via the values of a time-independent continuous level set function $\phi^f \in C^0(\Omega)$. More precisely, we suppose that

$$\begin{aligned} \Omega^0 &= \{x \in \Omega \mid \phi^f(x) \geq 0\} \\ \Omega^1 &= \{x \in \Omega \mid \phi^f(x) \leq 0\} \end{aligned} \quad (4)$$

2.1.2 Linear elasticity

If we assume that the two phases of the composite are linear elastic, time-independent and homogeneous, the stress functions $\sigma^{i,n}$ may be expressed as

$$\forall i \in \{0, 1\}, \quad \sigma^{i,n}(\nabla_s u^{i,n}) := C^i : \nabla_s u^{i,n} \quad \text{in } \Omega^i, \quad (5)$$

where $\nabla_s \cdot = \frac{1}{2}(\nabla \cdot + \nabla^T \cdot)$ and C^i is the fourth-order Hooke tensor of the material occupying phase i . This tensor may be expressed as a function of the the Lamé coefficients λ^i and μ^i as follows:

$$\forall i \in \{0, 1\}, \quad C^i : \nabla_s \cdot = \lambda^i \operatorname{Tr}(\nabla_s \cdot) \mathbb{I} + 2\mu^i \nabla_s \cdot \quad (6)$$

2.1.3 von Mises plasticity

Time continuous constitutive law. We consider the following von Mises plasticity model. The stress s in the material is given by

$$s = C : (\epsilon - \epsilon_p) \quad (7)$$

as a function of the strain ϵ (*i.e.* the symmetric part of the displacement gradient) and the plastic strain ϵ_p . The yield surface is defined as

$$f(s_D, q, p) = \sqrt{\frac{3}{2}(s_D - q) : (s_D - q)} - (Y_0 + R(p)) \quad (8)$$

where s_D denotes the deviatoric part of σ , p denotes the cumulative plastic strain and q the back stress. The flow rules are as follows:

$$\lambda \geq 0 \quad \lambda f(s_D, q, p) \quad f(s_D, q, p) \leq 0 \quad (9)$$

$$\begin{aligned} \dot{\epsilon}_p &= \lambda \left(\frac{s_D - q}{\|s_D - q\|} \right) \\ \dot{q} &= \lambda \left(\bar{H} : \frac{s_D - q}{\|s_D - q\|} \right) \\ \dot{p} &= \lambda \end{aligned} \quad (10)$$

where λ is the plastic multiplier, $R(p)$ is the isotropic hardening function, Y_0 is a constant yield parameter and H is a fourth-order kinematic hardening tensor. In our examples, \bar{H} will be vanishingly small (no kinematic hardening), and $R(p) = \hat{H}p$ (positive linear isotropic hardening).

Implicit time integration The previous ODE may be discretised in time using an implicit Euler scheme. This leads to the following semi-discrete material law.

$$\begin{aligned} \frac{1}{\Delta T} (C^{-1} : s^{n+1} - \epsilon^{n+1} + \epsilon_p^n) + \lambda \frac{s_D^{n+1} - q^{n+1}}{\|s_D^{n+1} - q^{n+1}\|} &= 0 \\ \frac{1}{\Delta T} (\bar{H}^{-1} : (q^{n+1} - q^n)) + \lambda \frac{s_D^{n+1} - q^{n+1}}{\|s_D^{n+1} - q^{n+1}\|} &= 0 \\ \lambda \geq 0 \quad \lambda f(s_D^{n+1}, q^{n+1}, p^n + \lambda \Delta T) \quad f(s_D^{n+1}, q^{n+1}, p^n + \lambda \Delta T) &\leq 0 \end{aligned} \quad (11)$$

Given $(\epsilon^{n+1}, \epsilon_p^n, q^n, p^n)$, the previous nonlinear system of equation (the last three constraints can be recast as a single nonlinear equality using the Heaviside function) can be solved for $(s^{n+1}, q^{n+1}, \lambda)$ using the usual combination of operator splitting and Newton iterative solution scheme. The update of internal variables are is performed according to

$$\begin{aligned} \epsilon_p^{n+1} &= \epsilon_p^n + \lambda \left(\frac{s_D^{n+1} - q^{n+1}}{\|s_D^{n+1} - q^{n+1}\|} \right) \Delta T \\ p^{n+1} &= p^n + \lambda \Delta T \end{aligned} \quad (12)$$

The procedure can therefore be summarised as an (implicit defined) relationship

$$s^{n+1} = s_{\Delta T}(\epsilon^{n+1}, (\epsilon_p^n, q^n, p^n); \mu, \Delta T) \quad (13)$$

where μ is a real-valued vector containing all the parameters of the constitutive law: Y_0 , all the free parameters of tensor \bar{H} and that of R).

Semi-discrete implicit stress functions At time $t_n > 0$, for any phase index $i \in \llbracket 1, 2 \rrbracket$ of the composite material, we may replace the elastic constitutive law by the following nonlinear function

$$\sigma^{i,n}(\nabla_s u^{i,n}) = s_{\Delta T}(\nabla_s u^{i,n}, \xi^{i,n-1}; \mu^i, \Delta T) \quad (14)$$

where the field of past internal variables $\xi^{i,n-1} = (\epsilon_p^{n-1}, q^{n-1}, p^{n-1})$ defined over Ω^i are sequentially and locally updated according to the procedure outlined above. We suppose that at the beginning of the simulation, all the internal variables are null.

2.2 Multiresolution problem in weak form

Keeping this in mind, we now split domain Ω arbitrarily into two non-overlapping domains: the coarse domain $\Omega^c =: \Omega^2$ and the fine domain Ω^f . Let us now redefine Ω^i as $\Omega^f \cap \Omega^i$, for $i \in \{0, 1\}$ (level set ϕ^f is unaffected by this change of notation). The interfaces between the domains

$$\begin{aligned} \Gamma^0 &= \Omega^0 \cap \Omega^1 \\ \Gamma^1 &= \Omega^0 \cap \Omega^2 \\ \Gamma^2 &= \Omega^1 \cap \Omega^2 \end{aligned} \quad (15)$$

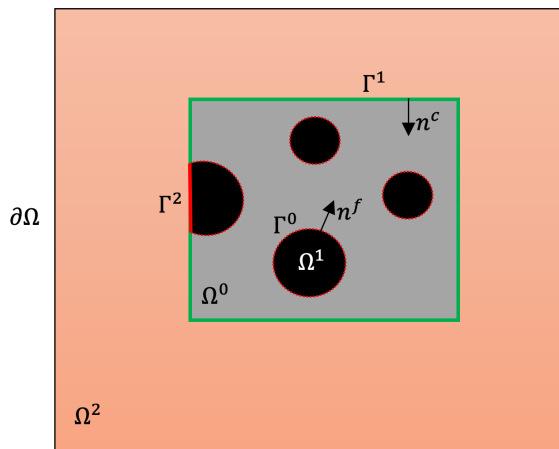


Figure 1: Domain partitioning for the multiscale method

In the coarse domain, we introduce a surrogate material model with slowly varying parameters in space. If the coarse material is elastic and homogeneous, it is characterized by constant tensor $C^c(x)$ (which may be obtained, for instance, via some form of homogenisation of the composite material), whose action reads as

$$C^c : \nabla_s \cdot = \lambda^c \text{Tr}(\nabla_s \cdot) \mathbb{I} + 2\mu^c \nabla_c \cdot \quad (16)$$

The resulting stress function is

$$\sigma^c(\nabla_s u^c) := C^c : \nabla_s u^c \quad \text{in } \Omega^c. \quad (17)$$

If the coarse material is plastic, we define the associated stress update at the n^{th} time increment, $n \in \llbracket 1 N \rrbracket$, by

$$\sigma^{c,n}(\nabla_s u^{c,n}) = s_{\Delta T}(\nabla_s u^{c,n}, \xi^{c,n-1}; \mu^c, \Delta T) \quad (18)$$

Now, the multiresolution problem of elasticity, at time $t_n \in \mathcal{T}_{\Delta T}$, is as follows. We look for a displacement field $u := \{u^0, u^1, u^2\} : \Omega^0 \times \Omega^1 \times \Omega^2 \rightarrow \mathbb{R}^D \times \mathbb{R}^D \times \mathbb{R}^D$ (u is overwritten to simplify the notations) satisfying

$$\sum_{i=0}^2 \int_{\Omega^i} \sigma^i(\nabla_s u^i) : \nabla_s \delta u \, dx = \sum_{i=0}^2 \int_{\Omega^i} f \cdot \delta u^i \, dx + \sum_{i=0}^2 \int_{\partial \Omega_t^i} t_d \cdot \delta u^i \, dx, \quad (19)$$

where

$$\forall i \in \{0, 1, 2\}, \quad \partial \Omega_t^i = \Omega^i \cap \partial \Omega_t \quad (20)$$

In the previous variational statement, arbitrary triplet $\delta u := \{\delta u^0, \delta u^1, \delta u^2\} : \Omega^0 \times \Omega^1 \times \Omega^2 \rightarrow \mathbb{R}^D \times \mathbb{R}^D \times \mathbb{R}^D$ is required to satisfy the homogeneous Dirichlet conditions

$$\forall i \in \{0, 1, 2\}, \quad u^i = 0 \quad \text{over } \partial \Omega_u^i := \partial \Omega_u \cap \partial \Omega^i \quad (21)$$

In the proposed multiresolution scheme, coarse domain Ω^c is defined as

$$\Omega^c = \{x \in \Omega \mid \phi^c(x) \leq 0\}, \quad (22)$$

where $\phi^c \in \mathcal{C}^0(\Omega)$ is a continuous level set function.

2.3 Discretisation of the multiresolution problem

2.3.1 Discretisation of the geometry

Let us introduce a coarse triangulation \mathcal{T}_H of domain Ω . The tessellated domain is denoted by Ω_H . Furthermore, let us introduce the finite element space of continuous piecewise linear functions, *i.e.*

$$\mathcal{Q}_H := \{w \in \mathcal{C}^0(\Omega_H) : w|_K \in \mathcal{P}^1(K), \forall K \in \mathcal{T}_H\} \quad (23)$$

We now define the finite element approximation of coarse domain Ω^c as

$$\Omega_H^c = \Omega_H^2 = \{x \in \Omega_H \mid \phi_H^c(x) \leq 0\} \quad (24)$$

where $\phi_H^c \in \mathcal{Q}_H$ is the coarse nodal interpolant of ϕ^c .

Let us now introduce a hierarchical subtriangulation \mathcal{T}_h of \mathcal{T}_H , with $h \ll H$. Due to the hierarchical structure, the union of all triangles of \mathcal{T}_h is the coarse finite element domain \mathcal{T}_H . We define space

$$\mathcal{Q}_{(H,h)} := \{w \in \mathcal{C}^0(\Omega_H) : w|_K \in \mathcal{P}^1(K), \forall K \in \mathcal{T}_h\} \quad (25)$$

With this definition, domains Ω^0 and Ω^1 are discretised as follows.

$$\begin{aligned} \Omega_{(H,h)}^0 &= \{x \in \Omega_H \mid \phi_H^c(x) \geq 0, \phi_h^f(x) \geq 0\} \\ \Omega_{(H,h)}^1 &= \{x \in \Omega_H \mid \phi_H^c(x) \geq 0, \phi_h^f(x) \leq 0\} \end{aligned} \quad (26)$$

We define the interface between the fine domains as

$$\Gamma_{(H,h)}^0 = \{x \in \Omega_H \mid \phi_H^c(x) \geq 0, \phi_{(H,h)}^f(x) = 0\} \quad (27)$$

and the interfaces between the coarse and the fine domains as

$$\begin{aligned}\Gamma_H^{fc} &= \{x \in \Omega_H \mid \phi_H^c(x) = 0\} \\ \Gamma_{(H,h)}^1 &= \{x \in \Gamma_H^{fc} \mid \phi_h^f(x) \geq 0\} \\ \Gamma_{(H,h)}^2 &= \{x \in \Gamma_H^{fc} \mid \phi_h^f(x) \leq 0\}\end{aligned}\tag{28}$$

Notice that finely discretized quantities are parametrised by a pair of mesh characteristics $\mathcal{H} = (H, h)$. this is due to the hierarchical structure of the multiresolution scheme that we have introduced (the coarse domain ‘‘overshadows’’ the composite material). To simplify the notations, the coarse sets and variables that only depend on H will also be written to be dependent on \mathcal{H} .

2.3.2 Overlapping domain decomposition

For the three different domains of the multiresolution scheme, we need to define appropriate extended domains. Such an extended domain is composed of all the elements that have a non-void intersection with its non-extended counterpart. Hence, the set of all elements of $\mathcal{T}_{\mathcal{H}}$ that have a non-zero intersection with $\Omega_{\mathcal{H}}^c$ is

$$\hat{\mathcal{T}}_{\mathcal{H}}^c := \{K \in \mathcal{T}_{\mathcal{H}} : K \cap \Omega_{\mathcal{H}}^c \neq \emptyset\}\tag{29}$$

The fictitious domain domain corresponding to this set is $\hat{\Omega}_{\mathcal{H}}^c := \bigcup_{K \in \hat{\mathcal{T}}_{\mathcal{H}}^c} K$. Similarly for the fine domains,

$$\forall i \in \{0, 1\}, \quad \hat{\mathcal{T}}_{\mathcal{H}}^i := \{K \in \mathcal{T}_{\mathcal{H}} : K \cap \Omega_{\mathcal{H}}^i \neq \emptyset\}\tag{30}$$

The domains corresponding to these sets are denoted by $\hat{\Omega}_{\mathcal{H}}^i := \bigcup_{K \in \hat{\mathcal{T}}_{\mathcal{H}}^i} K$, for $i = 0$ and for $i = 1$.

2.3.3 Extended interface FE spaces

We will look for an approximation $u_{\mathcal{H}} = (u_{\mathcal{H}}^0, u_{\mathcal{H}}^1, u_{\mathcal{H}}^2)$ of the multiresolution elasticity problem in space $\mathcal{U}_{\mathcal{H}} = \mathcal{U}_{\mathcal{H}}^0 \times \mathcal{U}_{\mathcal{H}}^1 \times \mathcal{U}_{\mathcal{H}}^2$, where

$$\begin{aligned}\mathcal{U}_{\mathcal{H}}^c &= \mathcal{U}_{\mathcal{H}}^2 := \{w \in \mathcal{C}^0(\hat{\Omega}_{\mathcal{H}}^c) : w|_K \in \mathcal{P}^1(K) \forall K \in \hat{\mathcal{T}}_{\mathcal{H}}^c\} \\ \forall i \in \{0, 1\}, \quad \hat{\mathcal{U}}_{\mathcal{H}}^i &:= \{w \in \mathcal{C}^0(\hat{\Omega}_{\mathcal{H}}^i) : w|_K \in \mathcal{P}^1(K) \forall K \in \hat{\mathcal{T}}_{\mathcal{H}}^i\}\end{aligned}\tag{31}$$

Notice that $u_{\mathcal{H}}$ is multi-valued in the elements that are cut by the two embedded interfaces. This feature allows us to represent discontinuities at the two interfaces.

The field of internal variables $\xi^{i,n}$, for any $n \in \llbracket 0, N \rrbracket$ and for any $i \in \llbracket 0, 2 \rrbracket$, will be defined over the corresponding approximated domain $\hat{\Omega}_{\mathcal{H}}^i$. These fields do not need to be extended to the fictitious domain.

2.3.4 Additional sets

We now define some additional sets, which is required to introduce the stabilisation strategy for our implicit boundary multiresolution formulation.

For stabilisation purpose, let us denote all elements which are intersected by $\Gamma_{\mathcal{H}}^{fc}$ by

$$\hat{\mathcal{G}}_{\mathcal{H}}^{fc} := \{K \in \mathcal{T}_{\mathcal{H}} \mid K \cap \Gamma_{\mathcal{H}}^{fc} \neq \emptyset\}\tag{32}$$

The domain corresponding to this set is denoted by $\hat{\Gamma}_{\mathcal{H}}^{fc} := \bigcup_{K \in \hat{\mathcal{G}}_{\mathcal{H}}^{fc}} K$. Similarly for the fine domains, for $i \in \{0, 1\}$,

$$\hat{\mathcal{G}}_{\mathcal{H}}^i := \{K \in \mathcal{T}_{\mathcal{H}} \mid K \cap \Gamma_{\mathcal{H}}^i \neq \emptyset\} \quad (33)$$

and the corresponding domains will be denoted by $\hat{\Gamma}_{\mathcal{H}}^i := \bigcup_{K \in \hat{\mathcal{G}}_{\mathcal{H}}^i} K$. We now define the set of Ghost-Penalty element edges for fictitious domain $\hat{\Omega}_{\mathcal{H}}^0$

$$\hat{\mathcal{F}}_{\mathcal{G}}^0 := \{F = K \cap K' : K \in \hat{\mathcal{T}}_{\mathcal{H}}^0 \text{ and } K' \in \hat{\mathcal{T}}_{\mathcal{H}}^0, F \cap \hat{\Gamma}_{\mathcal{H}}^0 \neq \emptyset\} \quad (34)$$

and for fictitious domain $\hat{\Omega}_{\mathcal{H}}^i$, $i \in \{1, 2\}$ as

$$\hat{\mathcal{F}}_{\mathcal{G}}^i := \{F = K \cap K' : K \in \hat{\mathcal{T}}_{\mathcal{H}}^i \text{ and } K' \in \hat{\mathcal{T}}_{\mathcal{H}}^i, F \cap \hat{\Gamma}_{\mathcal{H}}^i \neq \emptyset\} \quad (35)$$

2.4 Implicit boundary finite element formulation

The finite element multiresolution formulation is as follows: for any $\delta u_{\mathcal{H}} \in \mathcal{U}_{\mathcal{H}}$ satisfying the homogeneous Dirichlet boundary conditions,

$$a_{\mathcal{H}}(u_{\mathcal{H}}, \delta u_{\mathcal{H}}) + a_{\mathcal{H}}^{\sharp}(u_{\mathcal{H}}, \delta u_{\mathcal{H}}) + a_{\mathcal{H}}^{\heartsuit}(u_{\mathcal{H}}, \delta u_{\mathcal{H}}) = l_{\mathcal{H}}(\delta u_{\mathcal{H}}). \quad (36)$$

In the previous formulation, the bilinear form $a_{\mathcal{H}}$ is defined by

$$a_{\mathcal{H}}(u_{\mathcal{H}}, \delta u_{\mathcal{H}}) = \sum_{i=0}^2 \int_{\Omega_{\mathcal{H}}^i} \sigma^i(\nabla_s u_{\mathcal{H}}^i) : \nabla_s \delta u_{\mathcal{H}}^i dx. \quad (37)$$

and the linear form $l_{\mathcal{H}}$ is as follows:

$$l_{\mathcal{H}}(\delta u_{\mathcal{H}}) = \sum_{i=0}^2 \int_{\Omega_{\mathcal{H}}^i} f \cdot \delta u_{\mathcal{H}}^i dx + \sum_{i=0}^2 \int_{\partial\Omega_{\mathcal{H}}^i} t_d \cdot \delta u_{\mathcal{H}}^i dx, \quad (38)$$

Term $a_{\mathcal{H}}^{\sharp}$ is composed of terms that allows gluing the three domains together, using Nitsche's method. It is further expanded as

$$a_{\mathcal{H}}^{\sharp}(u_{\mathcal{H}}, \delta u_{\mathcal{H}}) = a_{\mathcal{H}}^{0;\sharp}(u_{\mathcal{H}}, \delta u_{\mathcal{H}}) + a_{\mathcal{H}}^{1;\sharp}(u_{\mathcal{H}}, \delta u_{\mathcal{H}}) + a_{\mathcal{H}}^{2;\sharp}(u_{\mathcal{H}}, \delta u_{\mathcal{H}}), \quad (39)$$

where the first term is for the interface between coarse and fine domains, while the second terms is for the interface between the matrix and the inclusions. We have that

$$\begin{aligned} a_{\mathcal{H}}^{i;\sharp}(u_{\mathcal{H}}, \delta u_{\mathcal{H}}) &= \beta^i \int_{\Gamma_{\mathcal{H}}^i} \llbracket u_{\mathcal{H}} \rrbracket^i \cdot \llbracket \delta u_{\mathcal{H}} \rrbracket^i dx \\ &- \int_{\Gamma_{\mathcal{H}}^i} \{t\}^i(u_{\mathcal{H}}) \cdot \llbracket \delta u_{\mathcal{H}} \rrbracket^i dx \\ &- \int_{\Gamma_{\mathcal{H}}^i} \{t\}^i(\delta u_{\mathcal{H}}) \cdot \llbracket u_{\mathcal{H}} \rrbracket^i dx. \end{aligned} \quad (40)$$

where

$$\begin{aligned} \llbracket u_{\mathcal{H}} \rrbracket^0 &= u_{\mathcal{H}}^1 - u_{\mathcal{H}}^2 \\ \llbracket u_{\mathcal{H}} \rrbracket^1 &= u_{\mathcal{H}}^0 - u_{\mathcal{H}}^2 \\ \llbracket u_{\mathcal{H}} \rrbracket^2 &= u_{\mathcal{H}}^0 - u_{\mathcal{H}}^1 \end{aligned} \quad (41)$$

denotes the jumps in the displacements across $\Gamma_{\mathcal{H}}^0, \Gamma_{\mathcal{H}}^1$ and $\Gamma_{\mathcal{H}}^2$ respectively; and $\{t\}^i$ denotes the following weighted averages

$$\begin{aligned}\{t\}^0 &= w_1^0 \sigma^1(\nabla_s u_{\mathcal{H}}^1) \cdot n_0 + w_2^0 \sigma^2(\nabla_s u_{\mathcal{H}}^2) \cdot n_0 \\ \{t\}^1 &= w_1^1 \sigma^0(\nabla_s u_{\mathcal{H}}^0) \cdot n_0 + w_2^1 \sigma^2(\nabla_s u_{\mathcal{H}}^2) \cdot n_0 \\ \{t\}^2 &= w_1^2 \sigma^0(\nabla_s u_{\mathcal{H}}^0) \cdot n_1 + w_2^2 \sigma^1(\nabla_s u_{\mathcal{H}}^1) \cdot n_1\end{aligned}\tag{42}$$

where $n_0 = -\frac{\nabla\phi^c}{|\nabla\phi^c|}$, $n_1 = -\frac{\nabla\phi^f}{|\nabla\phi^f|}$.

$$\begin{aligned}w_1^0 &= \frac{\frac{E^c}{H}}{\frac{E^1}{h} + \frac{E^c}{H}}, & w_2^0 &= \frac{\frac{E^1}{h}}{\frac{E^1}{h} + \frac{E^c}{H}} \\ w_1^1 &= \frac{\frac{E^c}{H}}{\frac{E^0}{h} + \frac{E^c}{H}}, & w_2^1 &= \frac{\frac{E^0}{h}}{\frac{E^0}{h} + \frac{E^c}{H}} \\ w_1^2 &= \frac{E^1}{E^0 + E^1}, & w_2^2 &= \frac{E^0}{E^0 + E^1}\end{aligned}\tag{43}$$

$$\begin{aligned}\beta^0 &= \frac{\frac{E^c}{H} \frac{E^1}{h}}{\frac{E^1}{h} + \frac{E^c}{H}}, \\ \beta^1 &= \frac{\frac{E^c}{H} \frac{E^0}{h}}{\frac{E^0}{h} + \frac{E^c}{H}}, \\ \beta^2 &= \frac{E^0 E^1}{h(E^0 + E^1)},\end{aligned}\tag{44}$$

Similarly for the interface between the matrix and the inclusions,

Finally, $a_{\mathcal{H}}^{\heartsuit}$ is an interior penalty regularisation term that reads as, for $i \in \{0, 1, 2\}$,

$$a_{\mathcal{H}}^{\heartsuit}(u_{\mathcal{H}}, \delta u_{\mathcal{H}}) = \sum_{F \in \mathcal{F}_G^i} \left(\int_F \beta^i \mathcal{H}^i \llbracket \nabla_s u_{\mathcal{H}} \rrbracket \llbracket \nabla_s (\delta u_{\mathcal{H}}) \rrbracket dx \right).\tag{45}$$

The nonlinear system of equations described above is solved by a standard Newton algorithm.

3 Numerical Results

This section first verifies the proposed multiresolution framework for a simplified multiscale elasticity problem. Then, we adopt von Mises material for the multiscale model and assess it for two types of hard and void micro-inclusions. Eventually, we assess the performance of a zoom with changing geometrical properties during the solution of nonlinear problems. All the numerical results are produced by the CutFEM library [24], developed in FEniCS [38].

3.1 Quasi-uniform porous structure

3.1.1 Verification test

In this section, the proposed multiresolution framework is assessed for a heterogeneous structure with micropores and then compared with a full microscale FEM model and a mixed multiscale method proposed in [36]. We consider the same quasi-uniform porous medium given in [36] which includes circular pores distributed all over the domain (as depicted in Figure 2). The material behaviour is assumed as elastic and isotropic. According to [36], the material properties for matrix are given as $E^0 = 1$ and $\nu^0 = 0.3$, and for the homogenized model are derived by Mori-Tanaka (MT) method [39, 40] as following: $E^2 = 0.78$ and $\nu^2 = 0.3$.

The computational meshes for the FEM and multiresolution models are shown in Figure 3a,b, which contain linear Lagrangian elements with the smallest element size of $h_{min} = 0.054$. The element size inside the zoom area is the same as in reference models for verification purposes. As shown for the discretized domain in Figure 4, the three types interfaces, $\Gamma_{(H,h)}^0$, $\Gamma_{(H,h)}^1$ and $\Gamma_{(H,h)}^2$ intersect the background mesh in an arbitrary fashion.

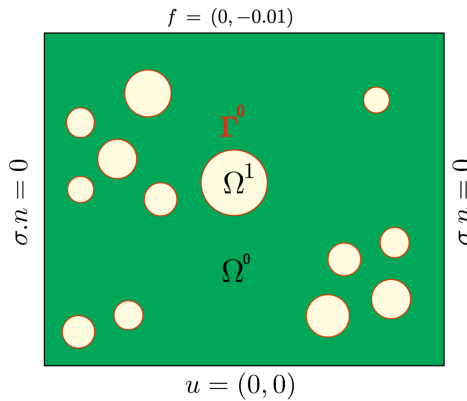


Figure 2: Boundary conditions and geometry of a heterogeneous structure with compression test

A compression test is conducted for the heterogeneous structure where the displacements are fixed along the x-direction and y-direction on the lower end, and force $f = (0, -0.01)$ is prescribed along the top edge. The FEM displacement component u_y contour is obtained and used as a reference solution, see Figure 5a. The same test is carried out for the multiscale model. The corresponding displacement field component is shown in Figure 5b. When our multiscale model is compared with the FEM and mixed multiscale models, a close similarity of u_y is observed inside the zooming region. Outside of the zoom, again, a satisfactory agreement is achieved.



Figure 3: Discretized domains; a) FE conforming mesh and b) CutFEM non-conforming mesh.

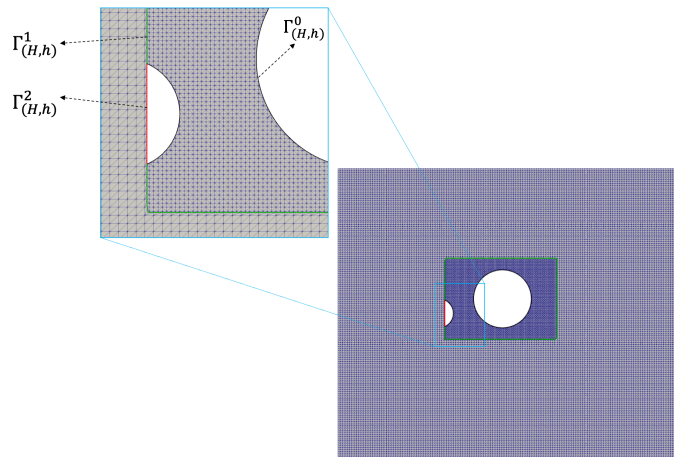


Figure 4: Discretized domain for the multiscale CutFEM including $\Gamma_{(H,h)}^0$, $\Gamma_{(H,h)}^1$ and $\Gamma_{(H,h)}^2$

We compute the stress field component σ_{yy} in Figure 6. Here again, a good agreement is achieved between the multiscale and reference models. The homogeneous model adopted in the coarse domain of the multiscale model smooth out the fluctuations produced by the coarse pores, and the overall trend in this domain is captured very well.

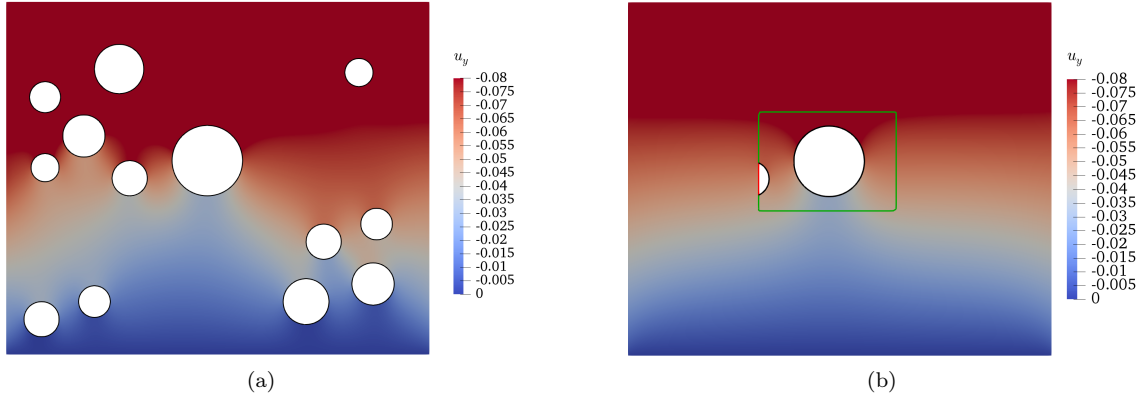


Figure 5: Displacement field component u_y ; a) FEM and b) Multiscale CutFEM.

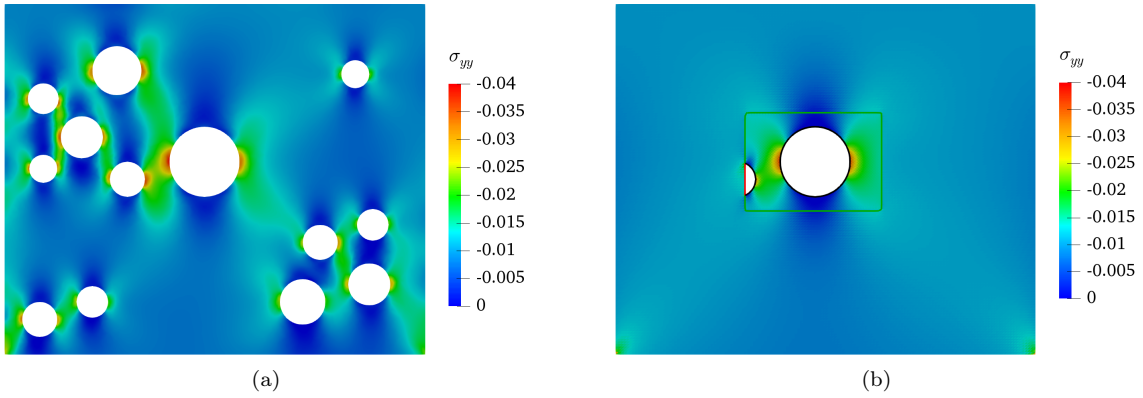


Figure 6: Stress field component σ_{yy} ; a) FEM and b) Multiscale CutFEM.

For further investigations, we study the effects of mesh coarsening in the coarse region of the multiresolution framework on the energy norm of the error field. The corresponding mesh layouts for the fine and coarse multiresolution models are depicted in Figures 3b and 7b, respectively. While the mesh outside the zoom is different for two multiresolution models, the mesh inside is considered the same size. Moreover, as shown in Figure 7a, a full fine resolution mesh is used for computation of the error field. We compute the energy norm of the error field with respect to the reference FE model according to the following formulation.

$$\|e\| = \sqrt{\int_{\Omega} \nabla_s e : \nabla_s e \, dx}. \quad (46)$$

where $e = u_{\text{ref}} - u$. u_{ref} and u denote the displacement for FE and multiresolution models, respectively. The corresponding energy norm for the two multiresolution models with respect to the reference FE model is computed in Figure 8. The results show that refining mesh outside of the zoom reduces the energy norm of the error field inside the zoom.



Figure 7: Computational meshes; a) Error field and b) multiresolution CutFEM with coarse mesh.

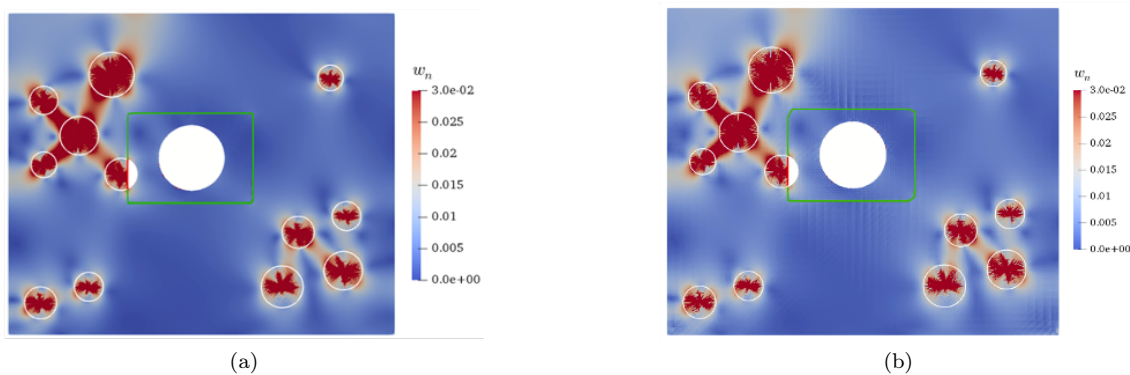


Figure 8: Energy norm of error field for Multiscale CutFEM; a) Fine mesh and b) Coarse mesh

3.2 S shape heterogeneous structure with a fixed zoom

In this section, we assess the ability and efficiency of the multiresolution CutFEM in modelling heterogeneous structures with nonlinear material properties and different types of heterogeneities. We consider an S shape heterogeneous structure with a random distribution of heterogeneities. As shown in Figure 9, the heterogeneities can be either voids or hard inclusions. We assume von Mises elastoplastic material behaviour for these structures. The material properties heterogeneous structures are: $2E^0 = E^1 = 2$, $\nu^0 = \nu^1 = \nu^2 = 0.3$, $\sigma_c^0 = \sigma_c^1 = \sigma_c^2 = 0.25$ and $\hat{H}_p^0 = \hat{H}_p^1 = \hat{H}_p^2 = 10^{-2}$. The material properties for the macroscale homogenized model with voids and inclusions are calculated by using MT as follows, respectively: $E^2 = 0.5, 1.3$. To analyze the influence of different microstructural features on the accuracy of the proposed multiscale framework, we consider the geometry and distribution of the voids and hard inclusions to be similar in the two structures. We restrict the displacement along the x and y directions on the lower end and apply force $f = (0, 0.18)$ incrementally on the top edge along the y-direction.

We employ two circular zooms fixed over a background mesh (see Figure 10). We refine the mesh inside the zoom regions with a refinement scale defined as $s = \frac{1}{16}$ (means each coarse element is subdivided hierarchically into 16 fine elements), where the largest element size is $h_{max} = 0.06$. The discretized physical domain of multiresolution models in Figures 10b,c show that all the three interfaces intersect the coarse background mesh (see Figure 10a) for both models in a fully arbitrary manner.

Next, we solve the nonlinear problem and assess the corresponding solution fields. The displacement field component u_y for two models in Figure 11 is smooth, especially in cut elements. Moreover, the stress field component σ_{yy} shown in Figure 12, is smooth for both structures. However, as expected, the structure with hard inclusion inherits more stiffness and absorbs more stresses inside and outside the zoom.

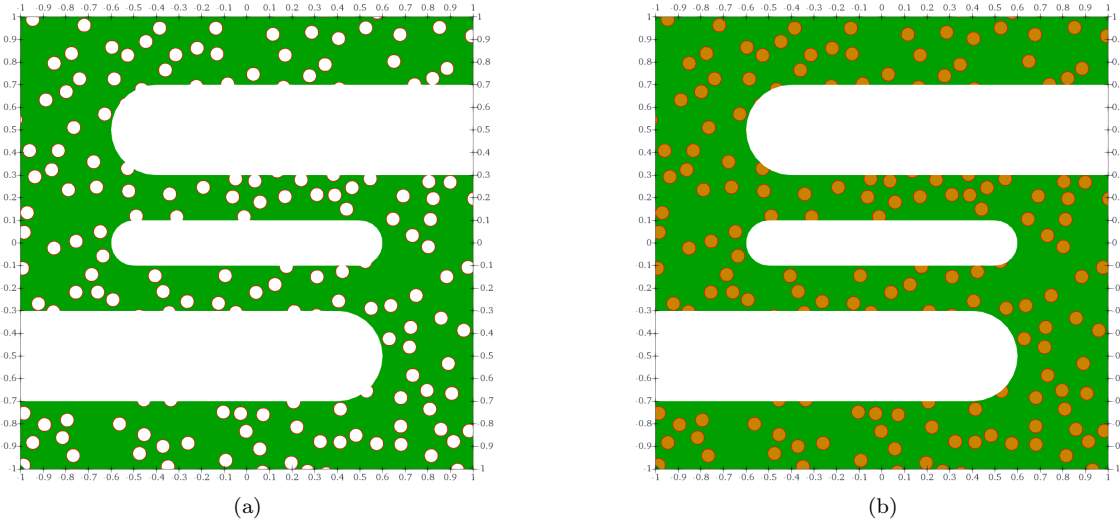


Figure 9: Geometry of the heterogeneous structures; a) heterogeneities are voids, b) heterogeneities are hard inclusions

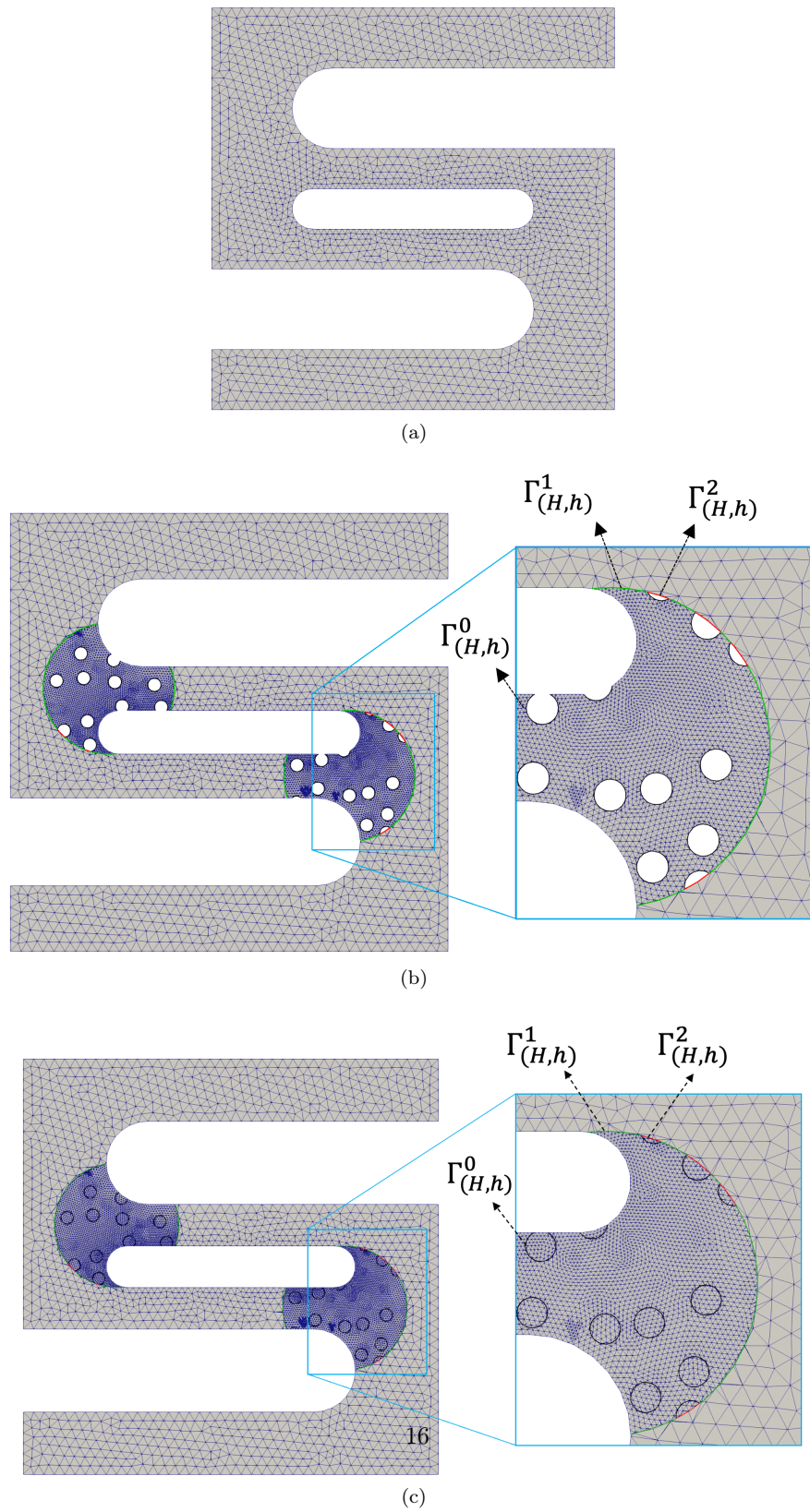


Figure 10: Computational meshes; a) coarse mesh, b) multiresolution mesh for the porous microstructure, c) multiresolution mesh for the microstructure with hard inclusions

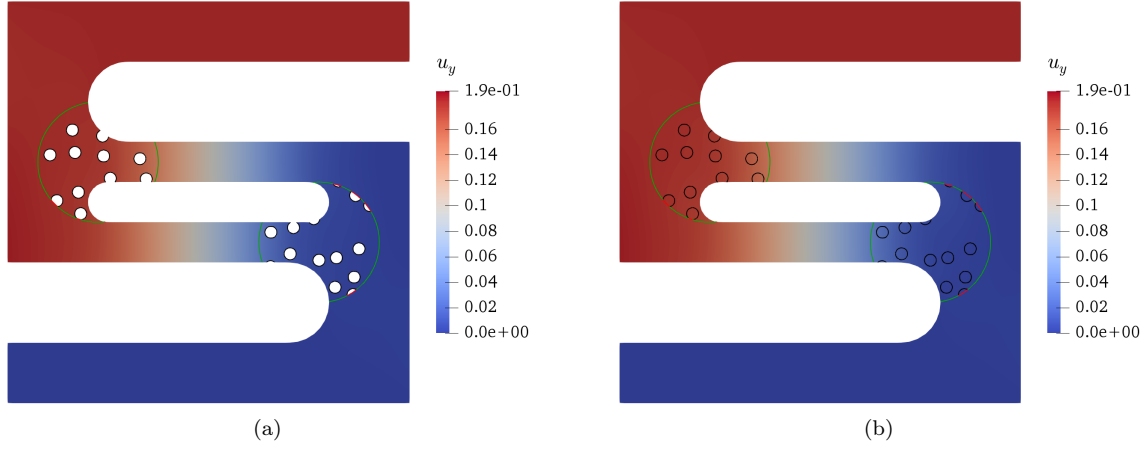


Figure 11: Displacement field u_y for the heterogeneous structures in the last time step; a) heterogeneities are voids, b) heterogeneities are hard inclusions

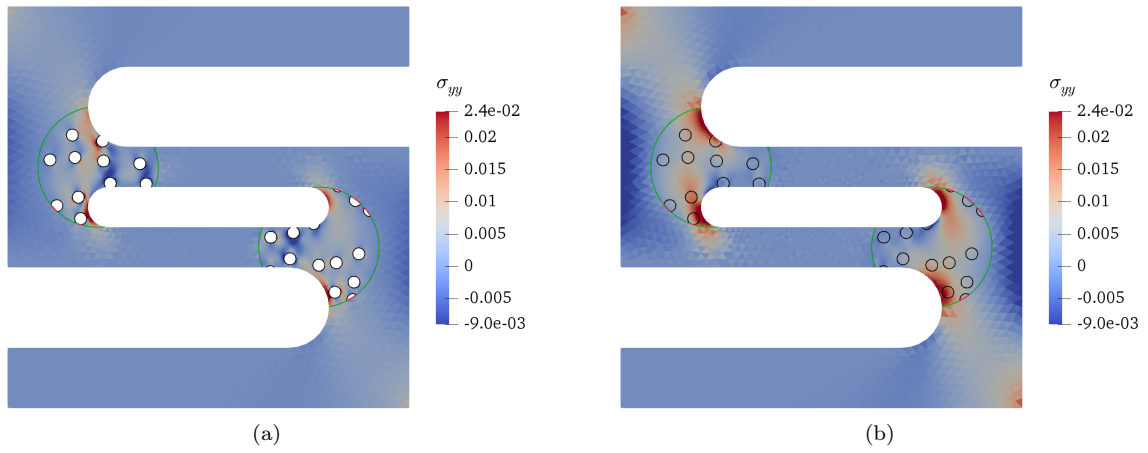


Figure 12: Stress component σ_{yy} for the last time step; a) heterogeneities are voids, b) heterogeneities are hard inclusions

3.3 S shape porous structure with a moving zoom

This section is devoted to the numerical study of a moving zoom for the proposed multiresolution with a von Mises plasticity material behaviour. We here consider the S shape microporous structure analyzed in section 3.2. However, contrary to the previous section, we will not fix the zooms over the background mesh but relocate them during the simulation. As shown in Figure 13, this relocation is carried out arbitrarily and independent of background mesh configuration. In this study, we change the location and size of zooming manually during the simulation to assess the numerical efficiency; however, using an adaptive approach would be more relevant from the physics point of view.

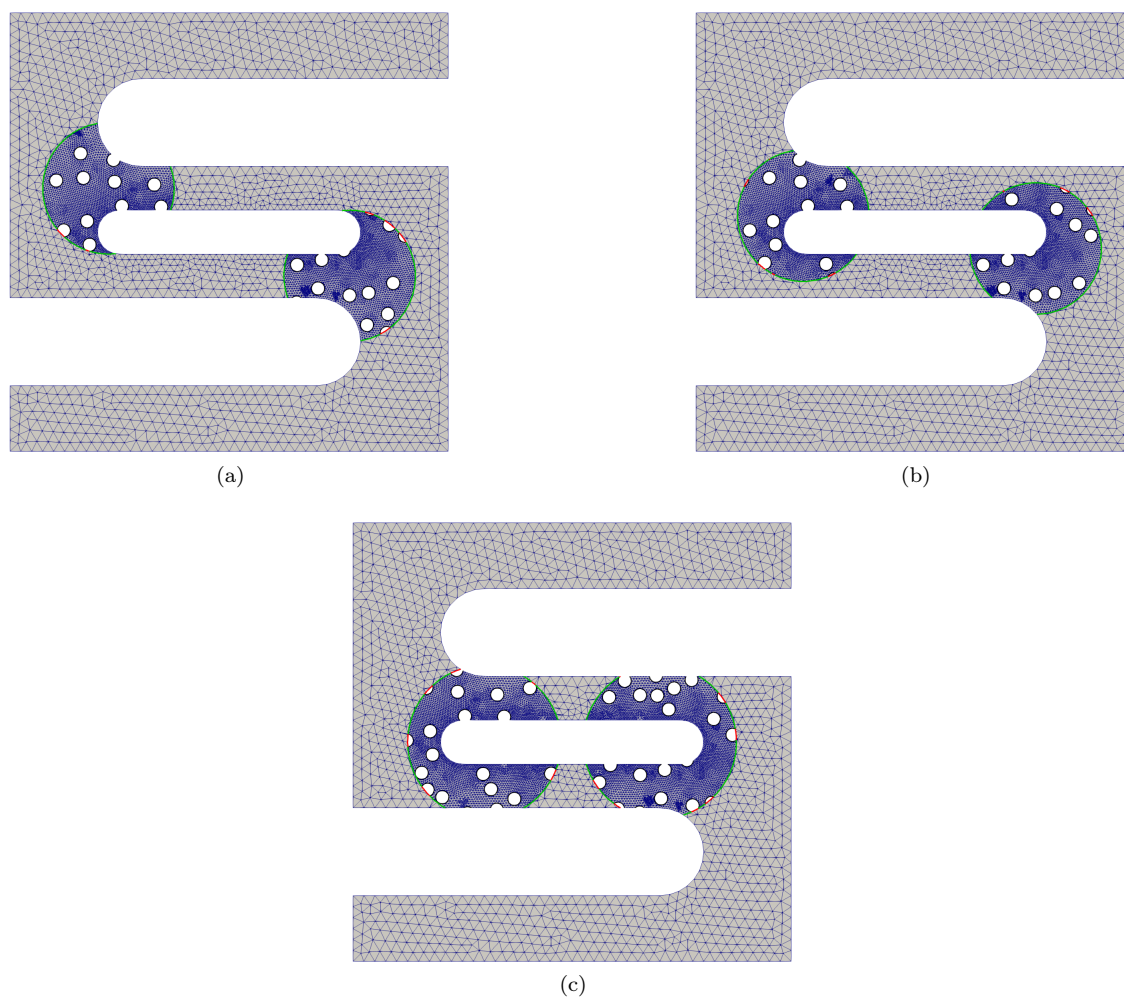


Figure 13: Computational meshes for the microporous heterogeneous structure with different set of zooms at various time steps

We show the displacement component u_y field for three different time in Figure 14. The results

show that the multiscale solution with a nonlinear material stays convergent in each time step, even with the relocation of the zooming region. Furthermore, the global behaviour during simulation stays smooth and without oscillations.

Next, we show the results in the form of plastic strain growth during the simulation. We compute the effective plastic strain at three-time steps and show the results in Figure 15. The changes in the zooms' location and size during the simulation are intended to capture the plastic strain growth.

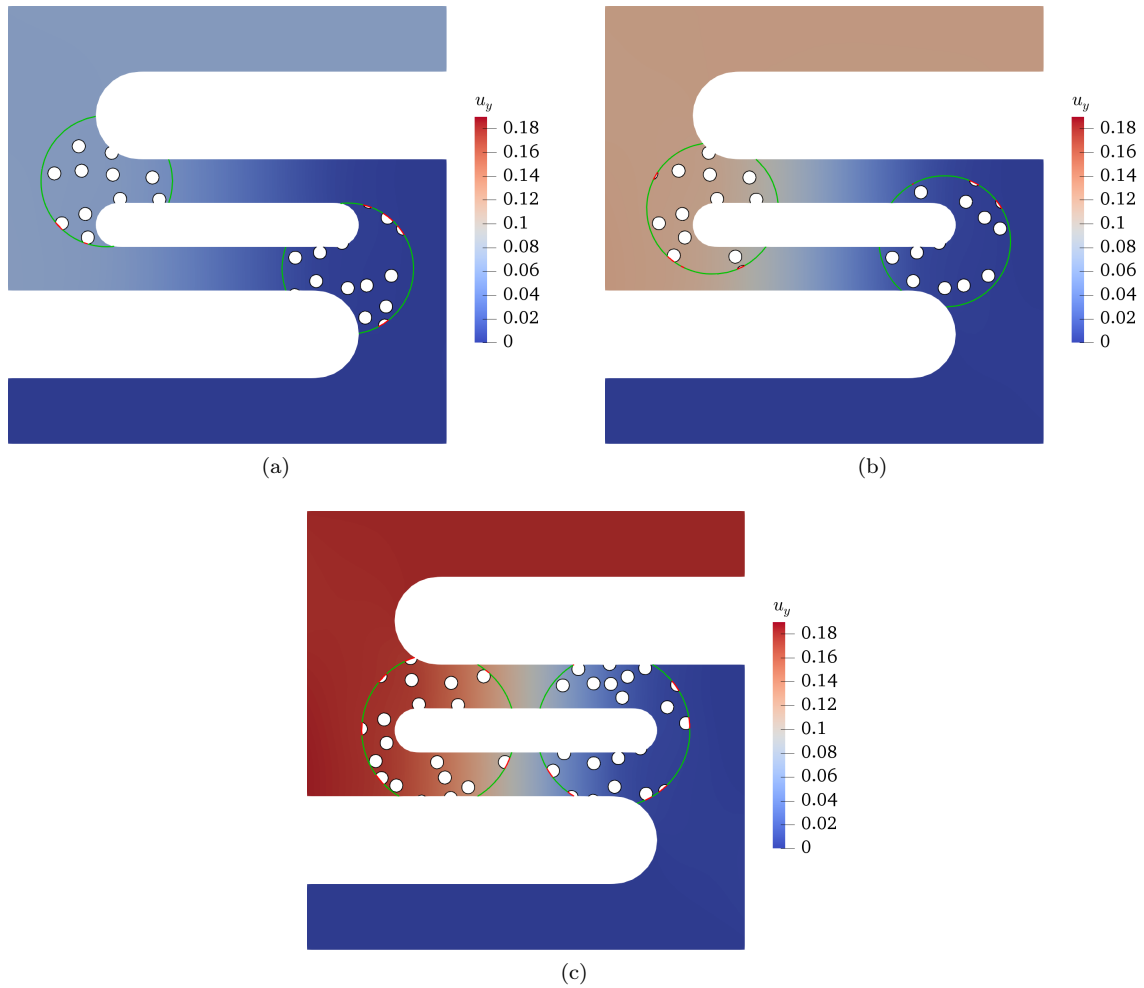


Figure 14: Displacement component u_y for the microporous heterogeneous structure with different set of zooms at various time steps

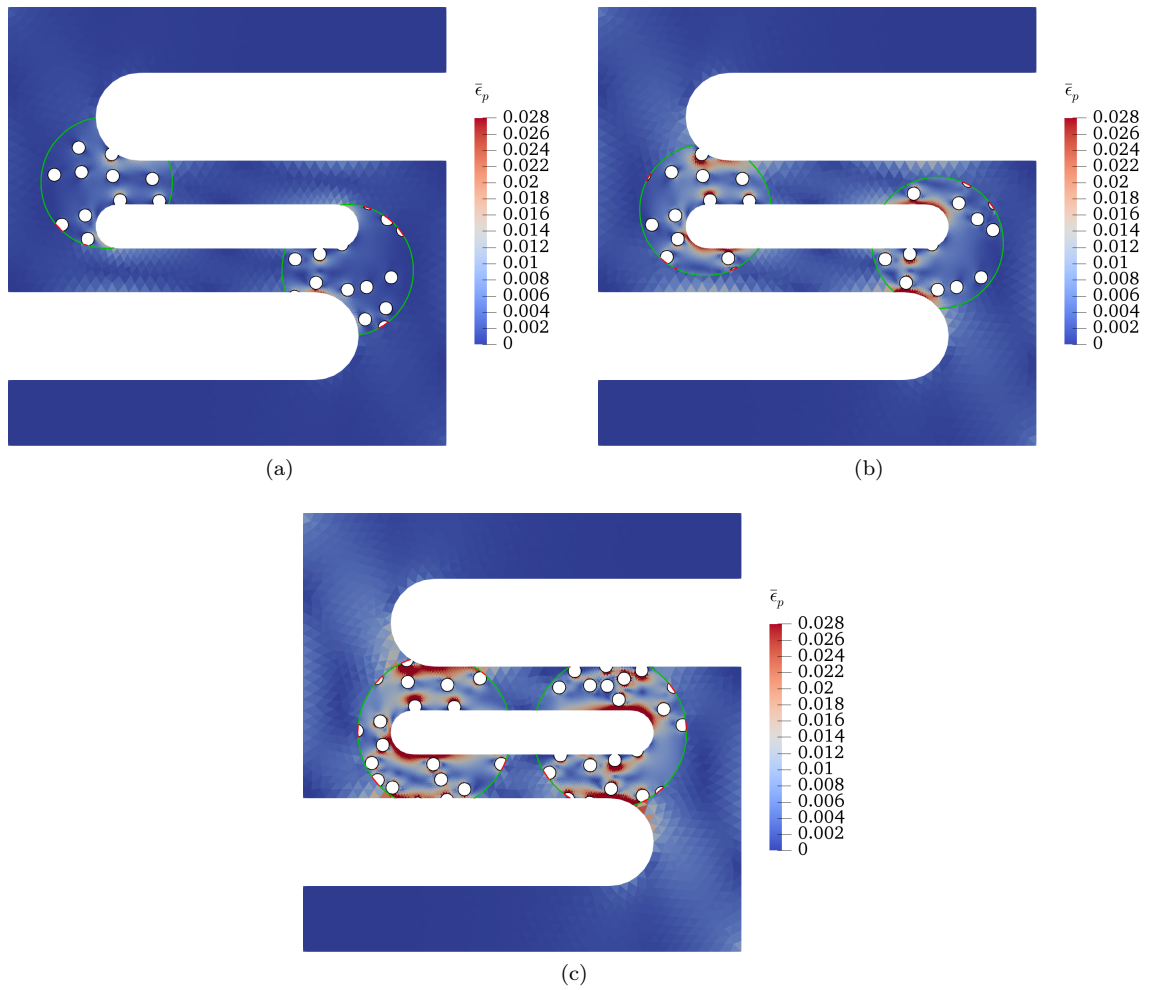


Figure 15: Effective plastic strain $\bar{\epsilon}_p$ at different time steps

4 Conclusions

A hierarchical multiresolution framework in the context of CutFEM has been developed for elastic and elastoplastic materials. Analytical distance functions have been exploited over the background mesh to define the zooming region and microstructure. The corresponding interfaces not only can intersect the background mesh in an arbitrary fashion but also are allowed to intersect each other freely. A full mesh independency in this framework is achieved by utilizing the ghost penalty regularization, which ensures the stability of cut elements. Furthermore, Nitsche's method has been exploited to enforce constraints over the interfaces between different regions, i.e. the interface between microscale and macroscale regions and the interface between matrix and inclusions.

The elements inside the zooming regions have been refined hierarchically for high-resolution analysis and then used for the interpolation of microstructure signed distance function. The corresponding results are compared with the counterpart FE models. For both models, linear Lagrangian elements are employed.

Three types of numerical examples have been assessed for the multiresolution framework: a fixed zoom for elasticity problems, a fixed zoom for plasticity problems and a moving zoom for plasticity problems. The first example is compared with the findings of a FEM as a reference model, and an excellent agreement is shown between the results. The results with the second example, which is applied for two types of inclusions (voids and hard inclusions) owning von Mises material, are satisfactory in terms of smooth distributions of global and local responses. Eventually, in the third example, the relocation of zooming regions during the solution of nonlinear problems has been assessed. The results showed that the zooming location could be changed successfully during the solution of a nonlinear system, which is a robust tool to apply for simulating propagation phenomena.

Acknowledgement

The authors acknowledges the support of Cardiff University, funded by the European Union's Horizon 2020 research and innovation program under the Marie Skłodowska-Curie grant agreement No. 764644.

References

- [1] Ellad B. Tadmor and Ronald E. Miller. *Modeling Materials: Continuum, Atomistic and Multiscale Techniques*. Cambridge University Press, 2011.
- [2] Pascale Kanoute, Daniela Boso, Jean-Louis Chaboche, and Bernhard Schrefler. Multiscale methods for composites: A review. *Archives of Computational Methods in Engineering*, 16:31–75, 2009.
- [3] Frédéric Feyel. A multilevel finite element method (fe2) to describe the response of highly non-linear structures using generalized continua. *Computer Methods in Applied Mechanics and Engineering*, 192(28):3233–3244, 2003. Multiscale Computational Mechanics for Materials and Structures.

- [4] T. Zohdi and P. Wriggers. A domain decomposition method for bodies with heterogeneous microstructure based on material regularization. *International Journal of Solids and Structures*, 36(17):2507–2525, 1999.
- [5] P. Raghavan and S. Ghosh. Concurrent multi-scale analysis of elastic composites by a multi-level computational model. *Computer Methods in Applied Mechanics and Engineering*, 193(6):497–538, 2004.
- [6] Shaoping Xiao and Ted Belytschko. A bridging domain method for coupling continua with molecular dynamics. *Computer Methods in Applied Mechanics and Engineering*, 193:1645–1669, 2004.
- [7] Ted Belytschko and Shaoping Xiao. Coupling methods for continuum model with molecular model. *International Journal for Multiscale Computational Engineering*, 1:115–126, 2003.
- [8] Ellad B. Tadmor, Michael Ortiz, and Rob Phillips. Quasicontinuum analysis of defects in solids. *Philosophical Magazine A*, 73(6):1529–1563, Jun 1996.
- [9] Lars A. Beex, Pierre Kerfriden, Timon Rabczuk, and Stephane Bordas. Quasicontinuum-based multiscale approaches for plate-like beam lattices experiencing in-plane and out-of-plane deformation. *Computer Methods in Applied Mechanics and Engineering*, 279:348–378, 2014.
- [10] Hachmi Ben Dhia. Multiscale mechanical problems: the arlequin method. *Comptes Rendus de l’Academie des Sciences Series IIB Mechanics Physics Astronomy*, 326:899–904, 1998.
- [11] Hashmi B. Dhia and Guillaume Rateau. The arlequin method as a flexible engineering design tool. *International Journal for Numerical Methods in Engineering*, 62:1442–1462, 2005.
- [12] Hachmi Ben Dhia. Further insights by theoretical investigations of the multiscale arlequin method. *International Journal for Multiscale Computational Engineering*, 6:215–232, 2008.
- [13] Paul T. Bauman, Hachmi Ben Dhia, Nadia Elkhodja, Tinsley Oden, and Serge Prudhomme. On the application of the arlequin method to the coupling of particle and continuum models. *Computational Mechanics*, 42:511–530, 2008.
- [14] Jacob Fish, Mohan A. Nuggehally, Mark S. Shepard, Catalin R. Picu, Santiago Badia, Michael L. Parks, and Hachmi Ben Dhia. Concurrent atc coupling based on a blend of the continuum stress and the atomistic force. *Computer Methods in Applied Mechanics and Engineering*, 196:4548–4560, 2007.
- [15] Bishnu P. Lamichhane and Barbara I. Wohlmuth. Mortar finite element for interface problems. *Computing*, 72:333–348, 2004.
- [16] Erik Burman and Peter Hansbo. Fictitious domain finite element methods using cut elements: I. a stabilized lagrange multiplier method. *Computer Methods in Applied Mechanics and Engineering*, 199(41):2680 – 2686, 2010.
- [17] H Ji and JE Dolbow. On strategies for enforcing interfacial constraints and evaluating jump conditions with the extended finite element method. *International Journal for Numerical Methods in Engineering*, 61(14):2508–2535, 2004.

- [18] Shaima M Dsouza, ALN Pramod, Ean Tat Ooi, Chongmin Song, and Sundararajan Natarajan. Robust modelling of implicit interfaces by the scaled boundary finite element method. *Engineering Analysis with Boundary Elements*, 124:266–286, 2021.
- [19] Erik Burman and Peter Hansbo. Fictitious domain finite element methods using cut elements: Ii. a stabilized nitsche method. *Applied Numerical Mathematics*, 62(4):328 – 341, 2012. Third Chilean Workshop on Numerical Analysis of Partial Differential Equations (WONAPDE 2010).
- [20] Ying Cai, Jinru Chen, and Nan Wang. A nitsche extended finite element method for the biharmonic interface problem. *Computer Methods in Applied Mechanics and Engineering*, 382:113880, 2021.
- [21] Thomas JR Hughes. *The finite element method: linear static and dynamic finite element analysis*. Courier Corporation, 2012.
- [22] Jean Donea, Antonio Huerta, J.-Ph. Ponthot, and A. Rodríguez-Ferran. *Arbitrary Lagrangian–Eulerian Methods*, chapter 14. John Wiley & Sons, Ltd, 2004.
- [23] Nicolas Moës, John Dolbow, and Ted Belytschko. A finite element method for crack growth without remeshing. *International Journal for Numerical Methods in Engineering*, 46(1):131–150, 1999.
- [24] Erik Burman, Susanne Claus, Peter Hansbo, Mats.G Larson, and Andre Massing. Cutfem: discretizing geometry and partial differential equations. *International Journal for Numerical Methods in Engineering*, 104:472–501, 2015.
- [25] Ronaldo I. Borja. A finite element model for strain localization analysis of strongly discontinuous fields based on standard galerkin approximation. *Computer Methods in Applied Mechanics and Engineering*, 190(11):1529–1549, 2000.
- [26] Jamshid Parvizian, Alexander Düster, and Ernst Rank. Finite cell method. *Computational Mechanics*, 41:121–133, 2007.
- [27] Susanne Claus and Pierre Kerfriden. A cutfem method for two-phase flow problems. *Computer Methods in Applied Mechanics and Engineering*, 348:185–206, 2019.
- [28] Thomas Frachon and Sara Zahedi. A cut finite element method for incompressible two-phase navier–stokes flows. *Journal of Computational Physics*, 384:77–98, 2019.
- [29] Peter Hansbo, Mats G Larson, and Sara Zahedi. A cut finite element method for coupled bulk-surface problems on time-dependent domains. *Computer Methods in Applied Mechanics and Engineering*, 307:96–116, 2016.
- [30] Susanne Claus, Samuel Bigot, and Pierre Kerfriden. Cutfem method for stefan-signorini problems with application in pulsed laser ablation. *SIAM Journal on Scientific Computing*, 40:1444–1469, 2018.
- [31] Sussane Claus and Pierre Kerfriden. A stable and optimally convergent latin-cutfem algorithm for multiple unilateral contact problems. *International Journal for Numerical Methods in Engineering*, 113:938–966, 2018.

- [32] Susanne Claus, Pierre Kerfriden, Faezeh Moshfeghifar, Sune Darkner, Kenny Erleben, and Christian Wong. Contact modeling from images using cut finite element solvers. *Advanced Modeling and Simulation in Engineering Sciences*, 8:1–23, 2021.
- [33] August Johansson, Benjamin Kehlet, Mats G. Larson, and Anders Logg. Multimesh finite element methods: Solving pdes on multiple intersecting meshes. *Computer Methods in Applied Mechanics and Engineering*, 343:672 – 689, 2019.
- [34] Jørgen S. Dokken, August Johansson, André Massing, and Simon W. Funke. A multimesh finite element method for the navier–stokes equations based on projection methods. *Computer Methods in Applied Mechanics and Engineering*, 368:113129, 2020.
- [35] August Johansson, Mats G. Larson, and Anders Logg. Multimesh finite elements with flexible mesh sizes. *Computer Methods in Applied Mechanics and Engineering*, 372:113420, 2020.
- [36] Ehsan Mikaeili, Susanne Claus, and Pierre Kerfriden. A mixed concurrent multiscale method via cutfem technology. *arXiv: 2111.03199*, 2021.
- [37] Erik Burman. Ghost penalty. *Comptes Rendus Mathématique*, 348:1217–1220, 2010.
- [38] Martin Alnæs, Jan Blechta, Johan Hake, August Johansson, Benjamin Kehlet, Anders Logg, Chris Richardson, Johannes Ring, Marie Rognes, and Garth Wells. The fenics project version 1.5. 3, 01 2015.
- [39] Toshio Mura. *Micromechanics of Defects in Solids*. Springer Netherlands, 1987.
- [40] Misagh Imani, Ali M. Goudarzi, Sayed Mahmood Rabiee, and Morteza Dardel. The modified mori-tanaka scheme for the prediction of the effective elastic properties of highly porous ceramics. *Ceramics International*, 44(14):16489 – 16497, 2018.